Front. Struc. Civ. Eng. 2012, 6(3): 321–333
DOI 10.1007/s11709-012-0161-y

RESEARCH ARTICLE

Development of an integrated structural health monitoring system for bridge structures in operational conditions

Xinqun ZHU[a*], Hong HAO[b]

[a] *School of Computing, Engineering and Mathematics, University of Western Sydney, Penrith, NSW 2751, Australia*

[b] *School of Civil and Resource Engineering, University of Western Australia, Crawley,WA 6009, Australia*

[*] *Corresponding author. E-mail: xinqun.zhu@uws.edu.au*

ABSTRACT This paper presents an overview of development of an integrated structural health monitoring system. The integrated system includes vibration and guided-wave based structural health monitoring. It integrates the real-time heterogeneous sensor data acquiring system, data analysis and interpretation, physical-based numerical simulation of complex structural system under operational conditions and structural evaluation. The study is mainly focused on developing: integrated sensor technology, integrated structural damage identification with operational loads monitoring, and integrated structural evaluation with results from system identification. Numerical simulation and its implementation in laboratory show that the system is effective and reliable to detect local damage and global conditions of bridge structures.

KEYWORDS integrated structural health monitoring, operational conditions, vibration and guided wave

1 Introduction

Civil engineering structures are subjected to environmental, service and accidental actions, which may cause damage to the structures. Regular inspection and condition assessment of engineering structures are necessary to determine their safety and reliability. Early damage detection and localization is vital for effective planning of maintenance and repair work. This would minimize the annual costs for maintenance and repair (~1.5% of initial value p.a. for bridges) and may help to avoid long out of service times that is usually associated with higher economic loss (e.g., traffic delay due to major bridge repair).

In recent years, structural health monitoring (SHM) has been increasingly recognized as a viable tool for improving the safety and reliability of structures. Many monitoring techniques have been reported in the literature by Doebling et al. [1], Sohn et al. [2], and Brownjohn [3]. These methods can be generally classified as either global or local. Global approaches are based on relatively low-frequency vibration measurements of the structure. The first few modes are used to assess the locations and the amount of damage. Vibration based condition monitoring has gained significant interest among researchers in recent decades, and a comprehensive literature review can be found in Doebling et al. [1], Carden and Fanning [4], Brownjohn [3], Fan and Qiao [5] and Brownjohn et al. [6]. Damage changes the dynamic response of structures, which may indicate the degradation of structural properties. However, damage is usually a local phenomenon (typically), and local response is captured by high frequency modes whereas low frequency modes tend to capture global response. It is even more difficult to identify damage by examining response-time histories directly, compounded by changes in excitation sources and/or environmental conditions. Also a common limitation of these techniques is that they require a high-fidelity model of the structure to start with. Local approaches are also called non-destructive evaluation (NDT) techniques. Conventional NDT is based on the regular visual inspection or localized methods using acoustic or ultrasonic, magnetic field, radiograph, eddy-current and thermal field principles. Chang and Liu [7] presented a literature review. While they can provide very useful information for decision-makers, these techniques require that the vicinity of the damage is

Article history: Received March 13, 2012; Accepted June 1, 2012

known a priori and that the portion of the structure being inspected is readily accessible. Recently, guided waves have been widely used for SHM and NDT. The guided wave (GW) based methods generate a fairly high frequency pulse to the structure, which make minor damage detection become possible. GW can be defined as stress waves forced to follow a path defined by the material boundaries of a structure. Due to its capacity of relatively long propagation range as well as its flexibility in selecting sensitive mode-frequency combinations, GW has been found as an effective and efficient way to detect incipient of damages in civil, mechanical and aerospace structures recently. Raghavan and Cesnik [8] presented a literature review for GW based structural health monitoring. The majority of research has focused on damage sources such as delamination, low velocity impact and debond in sandwich and stiffened CFRP structures [9,10]. The piezoelectric materials are widely used for exciting and measuring GWs in SHM. With the use of built-in actuators and sensors, the GW based approach is complementary to the development of integrated systems for continuous online monitoring [11].

In addition to the extensive research efforts conducted separately in global and local SHM, integration of these two technologies is desired. An integrated health monitoring technique was developed to detect and locate structural damage using structural impedance sensors [12]. The impedance-based method is combined with a model-based identification technique using wave propagation approach. A damage index approach based on high frequency wave propagation data and low frequency vibration measurements is developed to detect the damage in structural components by Banerjee et al. [13]. Ratnam et al. [14] presented a combined finite-element model and Lamb wave propagation parameter method for structural health monitoring. It was used to identify the damage in a cantilever plate successfully. Zhang et al. [15] developed an integrated framework for building structures. The system identification was embedded in the procedure of reliability evaluation of stochastic building structures. Ling and Mahadevan [16] presented a Bayesian probabilistic method to integrate model-based fatigue damage prognosis with structural health monitoring data. Wang and Hao [17] presented an integrated structural health monitoring scheme by combining the guided wave based and vibration monitoring. The efficiency and reliability of the combination method in damage identification has been demonstrated using experimental results of RC structures.

In this paper, the vibration-based global approach is integrated with the guided wave based local technique. The global health monitoring is to check the changes of the global properties and the local NDT is to determine the nature of damage. Some of the recent research activities related to SHM to develop an integrated structural health monitoring system are presented. It includes developing sensor technologies for localized damage detection, vibration-based global condition monitoring and using this information to evaluate the load carrying capacity for existing bridge structures. Numerical simulation and its implementation in laboratory show that the system is effective and reliable to detect local damage and global conditions of bridge structures.

2 Embedded sensor techniques—integrated smart materials with structures

2.1 Guide wave based SHM

The guided wave based SHM system [18], shown in Fig. 1, includes two parts: a) the actuating part is to provide the excitation or input of the system. It includes the actuator of piezoelectric strips and the power amplifier that provides the power supply of the actuator. b) The piezo sensing part is to measure the response. This part includes the piezo film element and its charge amplifier.

The actuators were mounted on the surface of the steel reinforcing bar with Araldite Kit K138 and the steel bars were cast into a concrete slab to evaluate the delamination between the steel bars and concrete. The stripe actuators from APC International, Ltd. are selected as actuators in this study. The actuator includes two thin strips of piezoelectric ceramic that are bonded together with the direction of polarization coinciding and are electrically connected in parallel. When electrical input is applied, one ceramic layer expands and the other contracts, causing the actuator to flex. In this study, only one ceramic layer is applied the electrical input so that it will generate the wave. NI USB-6251 is used to provide the short-time Morlet wavelet for actuating the structure by a linear power amplifier. The frequency and the number of waves can be adjusted to optimize the wave propagation along the steel bars.

The DT1 series piezo film elements from Measurement Specialties, Inc. are selected as the sensors. The sensors are also glued to the steel bars with Araldite Kit K138. Signals from sensors are collected by a data acquisition system based NI PCI-6133. The sampling frequency of the system is up to 2MHz. A program based on Labview is developed to control NI USB-6251 and 2 NI PCI-6133 working simultaneously.

2.2 Debonding detection of RC structures

A reinforced concrete slab (1500 mm × 500 mm × 100 mm), shown in Fig. 2, is constructed for debond tests in the laboratory. The slab is supported at two ends and includes five reinforcement bars (round bar with a diameter of 16 mm) with 50 mm cover of concrete to reduce the effect of the concrete thickness. The distance between two rebars is about 100 mm. The strength of the rebars is 250 MPa. The slab was covered in plastic the following day after pouring

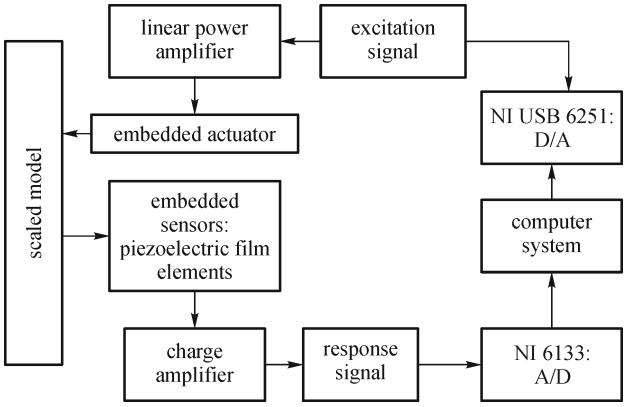

Fig. 1 Guided wave based SHM system scheme

the concrete and then the formwork was stripped after 14 days in compliance with the code requirement stated in AS36610 clause 19.6.2.5. The concrete cylinders for the slab were tested after 28 days and had an average compressive strength of 40.2 MPa. The Young's modulus of the slab is 3.3×10^{10} Pa and the density is 2450 kg/m^3. Different debond sizes between the reinforcement bar and concrete, b = 0 mm, 21 mm, 37 mm, 58 mm and 99 mm, are simulated. The debond is simulated by a plastic tube sealed at two ends so that the concrete cannot enter the tube during the construction. One actuator and four piezo film elements at different locations (400 mm, 600 mm, 800 mm and 1000 mm) are mounted on the surface of the reinforcement bar without debond, and other rebars are with one actuator and two piezo film elements at 400 mm and 1000 mm, respectively.

Two parameters are changed when the wave propagates along the steel bar in or out of concrete: the wave speed and the response signal's amplitude. The speed of the wave propagation along the steel bar in concrete are related to the property of the interface between steel bars and concrete. Measurements of the wave speeds using the embedded piezoelectric sensors provide a technique to assess the delamination in the interface. Supposing that the distance between the tip of actuator and the tip of the receiver is L and the time for the wave to travel this distance is t, the average speed of the wave is $v = L/t$. If the wave speeds along the steel bar only or in concrete without delamination are v_s and v_c, respectively, the scalar parameter can be defined as follows:

$$\alpha_{\text{speed}} = 1 - \frac{v - v_c}{v_s - v_c}, \tag{1}$$

where α_{speed} is a scalar parameter. $\alpha_{\text{speed}} = 0$ corresponds to the wave propagation along the steel bar only. $\alpha_{\text{speed}} = 1$ is for the steel bar in concrete without delamination.

The signal's amplitude is another parameter to be affected by the interface between steel bars and concrete. When the wave travels through a medium, its intensity diminishes with the distance. Attenuation that includes the combined effect of scattering and absorption is defined by a decay rate of wave as it propagates through material. For a single frequency wave, the amplitude change of a decaying plane wave can be expressed as

$$A_w = A_{w0} e^{-\alpha x}, \tag{2}$$

where A_{w0} is the amplitude of the wave at the actuating point and A_w is the reduced amplitude after the wave has traveled a distance x from the initial location. α is the attenuation coefficient of the wave traveling in the x-direction.

Similar to the scalar parameter α_{speed}, there is another parameter corresponding to the changes of the signal's amplitude

$$\alpha_{\text{amplitude}} = 1 - \frac{A_w - A_{wc}}{A_{ws} - A_{wc}}, \tag{3}$$

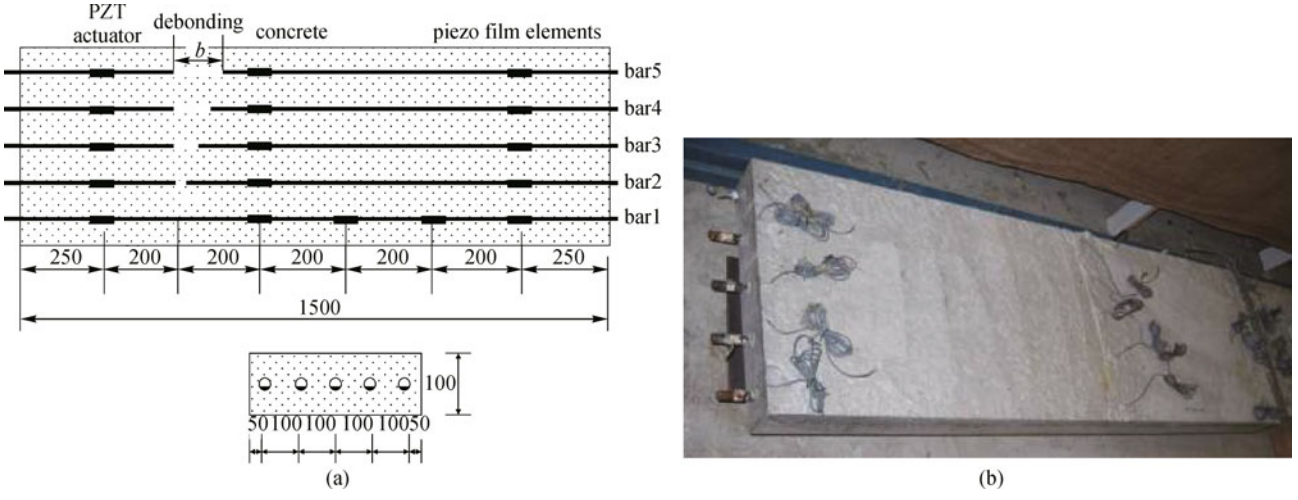

Fig. 2 Experimental model

where A_{ws}, A_{wc} are the signal's amplitudes for wave propagation along the steel bars only or in concrete without delamination, respectively. $A_{amplitude} = 0$ indicates that there is no concrete around the steel bar. Otherwise, the steel bar is in the concrete without delamination in the interface.

Figure 3 shows the values of two scalar parameters for the rebars with different debonding lengths. The experimental results show that there is an approximate linear relationship between the parameters and the debond length. The scalar speed parameter reduces with the debond length and the amplitude parameter increases. These two parameters could be good indicators of debonding damage.

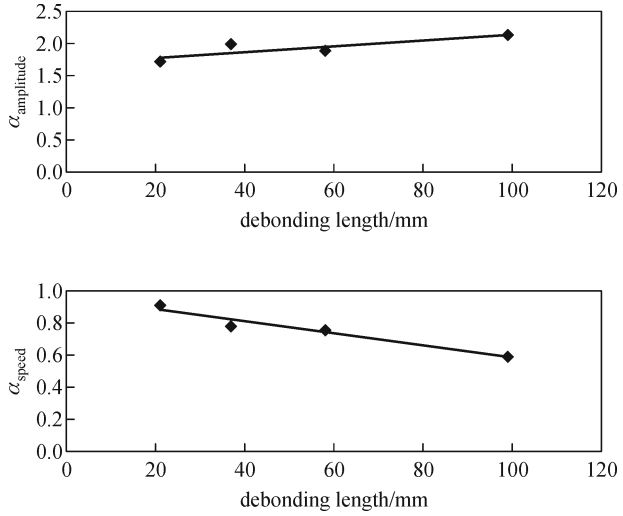

Fig. 3 Experimental results

2.3 Spectral element model for debonding damage

To further study the wave propagation along the rebar in the concrete, a concrete-steel interface spectral element is developed and scalar damage parameters characterizing changes in the interface (debonding damage) are incorporated into the formulation of the spectral element that is used for damage detection of reinforced concrete structures [19]. Through the bond, concrete and steel can work together. But in reality, concrete will not deform uniformly over the cross section. Only the concrete near the steel bar will have similar deformation with the steel rebar, and the deformation decreases along the cross section away from the steel bar toward the concrete surface. Therefore, the axial deformation of the concrete beam is not uniform over the cross section. Based on the axial deformation assumption and stress equilibrium, an equivalent area A_c is then defined, which can be obtained from the wave speed. Since the damping ratio η is very small, the wave speed along the steel rebar in concrete can be represented as follows

$$c = \sqrt{\frac{EA}{\rho A}} = \sqrt{\frac{E_s A_s - E_c A_c}{\rho_s A_s + \rho_c A_c}}, \tag{4}$$

where E_s, E_c denote the Young's modulus of the steel and concrete. A_s and A_c are the areas of the cross-sections corresponding to the steel and concrete, respectively. ρ_s, ρ_c are the densities of the steel and concrete. The equivalent concrete cross sectional area can be calculated by

$$A_c = \frac{E_s - \rho_s c^2}{E_c + \rho_c c^2} A_s, \tag{5}$$

In practice, c can be measured easily. Based on Eq. (5), A_c can be obtained, and the following equivalent parameters are defined

$$E = E_{eq} = \frac{E_s A_s - E_c A_c}{A},$$

$$\rho = \rho_{eq} = \frac{\rho_s A_s + \rho_c A_c}{A},$$

$$\eta = \eta_{eq} = \frac{\eta_s A_s + \eta_c A_c}{A}, \tag{6}$$

where $A = A_{eq} = A_s + A_c$. η_s, η_c are the viscous damping ratios of the steel and concrete, which are used to simulate the material damping.

In the proposed SEM, A_c is the variable which can provide some indications of debonding damage. In this study, the debonding damage index and conventional damage indices are defined as follows:

$$\alpha_b = 1 - \frac{A_c'}{A_c},$$

$$\alpha_s = 1 - \frac{E_s'}{E_s},$$

$$\alpha_c = 1 - \frac{E_c'}{E_c}, \tag{7}$$

where A_c' is the unknown real effective area of concrete. E_c', E_s' are the damaged elastic moduli for concrete and steel respectively. When there is neither debonding nor damage to concrete and steel rebar, $A_c' = A_c$, $E_c' = E_c$, $E_s' = E_s$ and $\alpha_b = \alpha_c = \alpha_s = 0$. When full debonding occurs, $A_c' = 0$, or full damage to concrete or steel rebar, $E_c' = 0$, $E_s' = 0$, then $\alpha_b = \alpha_c = \alpha_s = 1$. In other cases, $0 < \alpha_b, \alpha_c, \alpha_s < 1$.

To study the feasibility of GW-based damage identification of debonding damage in RC structures, the effect of different debonding damage on the received wave is studied using the proposed numerical model. The above parameters of the test model are used in the calculation. Three parameters, namely debonding length, location and

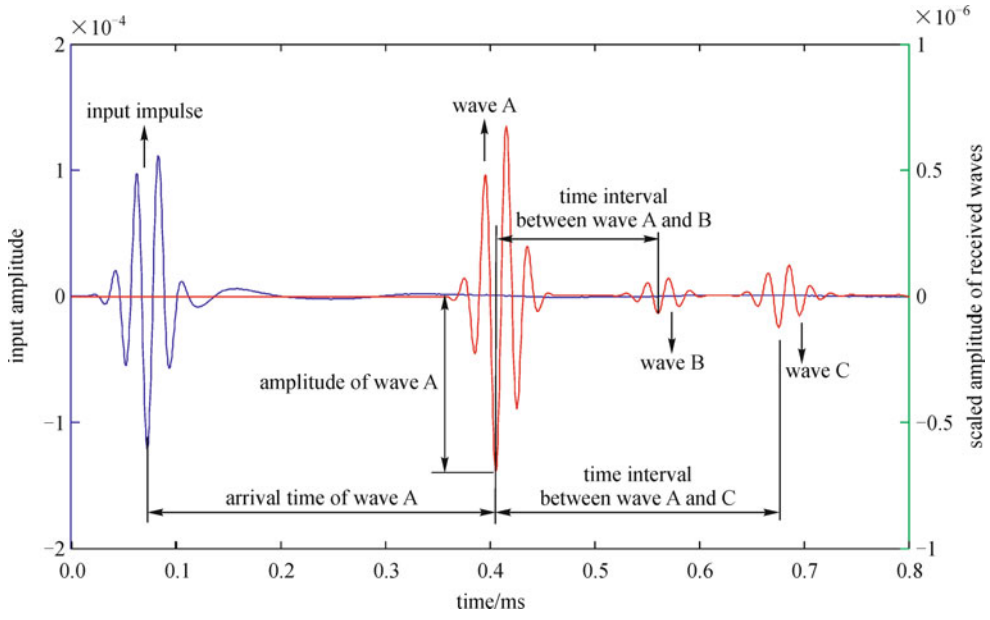

Fig. 4 Illustration of received waves and the corresponding parameters

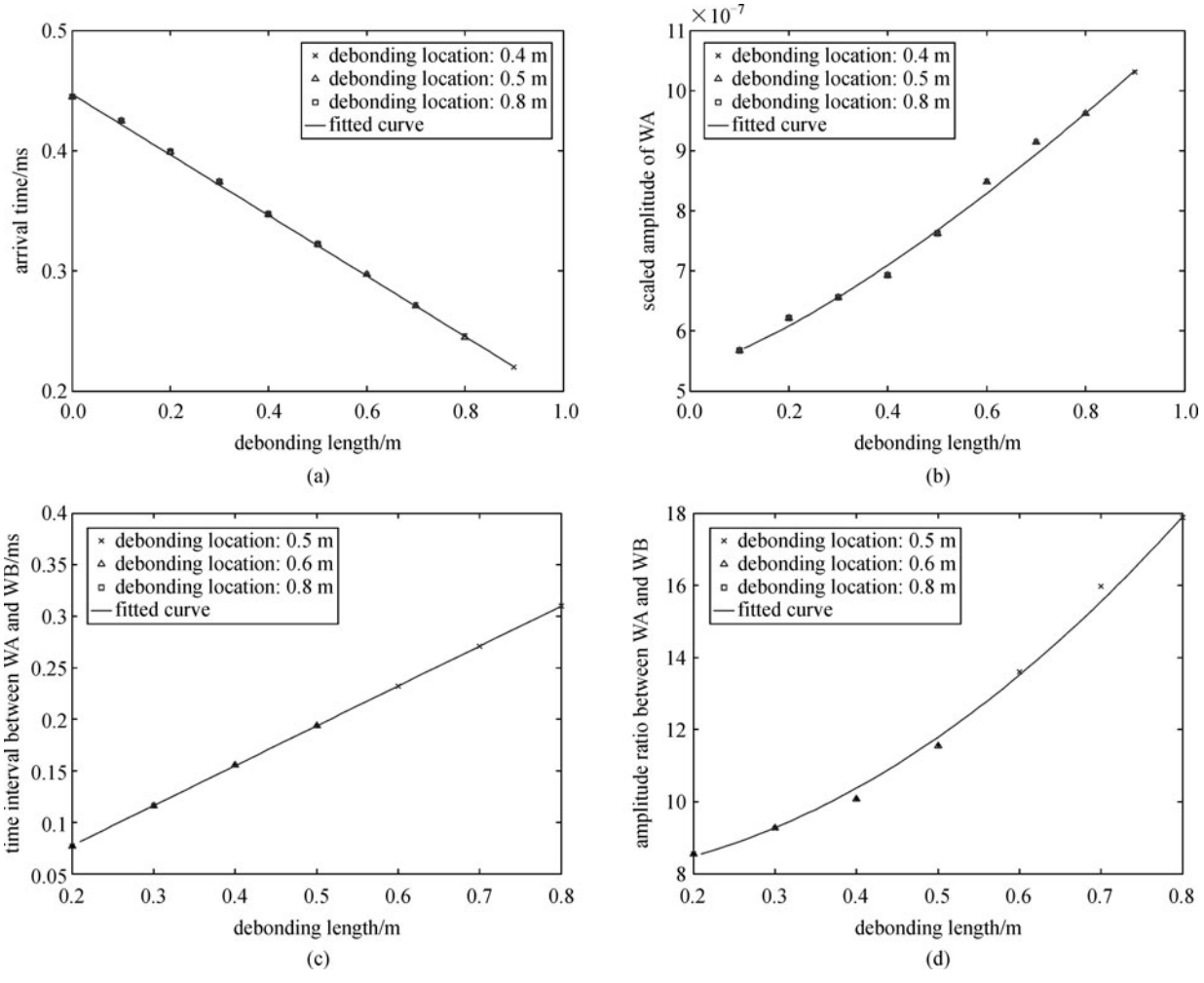

Fig. 5 Relationship between the debonding length and the four parameters

level, are used to describe the debonding damage. The debonding level is defined as a debonding damage index in Eq. (7) by the real effective area of concrete around the steel bar. The debonding damage zone is defined as a damaged element. The debonding length and location correspond to the length and location of the damage element. Different debonding damage scenarios are simulated by changing the debonding length, location and level. The effect of damage in concrete or steel bar on waveform is also investigated by changing the damage indices α_c, α_s in the element.

Guided-wave propagation along the steel bar buried in concrete is very complicated. Figure 4 shows a typical wave propagation process from the input signal to the response. There are three waves, namely Wave A, B and C in the figure. Wave A is the main incident wave propagated from the wave source. Wave B and C are additional waves caused by debonding damage. In this study, four parameters are used to describe the changes in the waveform due to the damage. The arrival time of Wave A is defined as the time interval between the input signal and Wave A. This parameter is used to describe the time delay of Wave A, which is related to the wave speed directly. The amplitude of Wave A is the second parameter to describe the attenuation of wave propagation in the material. The time interval between Wave A and B or Wave A and C is used to describe the time delay of Wave B or C. The amplitude ratio of Wave A to B or Wave A to C is used to describe the amplitude properties of Wave B or C. In the above, the amplitude of the wave is defined as the absolute peak value. The changes of these parameters due to the damage and their sensitivity to damage are studied in the following.

Since A_c changes with the interface condition, it can provide some indications of debonding damage. The above parameters of the test model are used in the calculation. Three parameters, namely debonding length, location and level, are used to describe the debonding damage. The 5-spectral element model is used in the calculation. The third element is taken as the damaged element and the debonding damage is assumed as the full debond of the element. Both the debonding length and location are varied in numerical calculations. Figure 5 shows the relationship between the four parameters and the debonding length when the debonding damage occurs at different locations.

The results show that the debonding location has no obvious effect on the arrival time, the amplitude of Wave A, and the time interval and the amplitude ratio between Wave A and B. But all these parameters depend on the debonding length, the analytical relationships between debonding lengths, and these parameters are derived based on the numerical simulation results. These relationships can be used as indicators to quantify the debonding length.

Based on the above discussions, the guided wave based approach can be used to detect the local damage and the nature of the damage. The key components of the bridge could be monitored using this approach, and the results such as the debonding damage could be integrated into the finite element model to predict the bridge overall loss of stiffness and load carrying capacity. This will be further studied in the next step.

3 Integrated structural damage identification with operational loads monitoring

3.1 Vibration-based SHM in operational conditions

System identification technique is used widely in the damage assessment of engineering structures. It is regarded as the key part of a structural health monitoring system, which identifies the physical parameters from the raw measurement data. The changes in the identified parameters will be used to assess the damage of the structure. Most system identification methods need the input loading and output response information. However, the input excitations, such as wind forces, traffic or earthquake loads are usually unknown or difficult to be accurately measured under actual operating conditions. This is particularly true for large civil engineering structures such as buildings, long bridges and offshore structures. System identification techniques using measured structural responses only to identify model or structural parameters invoked great interests in the past few decades.

One of the questions that attract significant research attention is related to the use of structural response from operational dynamic loads in the damage detection procedures. Previous studies are mainly on the problem of modal testing and analysis of structures under operational loads. Law and Zhu [20] presented an overview of damage models and algorithms for assessment of structures under operational conditions. In case of highway bridges, operating vehicle could be utilized to reduce the number of measuring devices [21–25]. Here the bridge condition assessment under traffic conditions is presented as an example [26]. For a vehicle-bridge system, the equations of motion of the bridge under moving vehicular loads can be written as follows

$$\mathbf{M}_b\ddot{\mathbf{u}} + \mathbf{C}_b\dot{\mathbf{u}} + \mathbf{K}_b\mathbf{u} = \Phi\mathbf{P}, \tag{8}$$

where $\mathbf{M}_b$, $\mathbf{C}_b$ and $\mathbf{K}_b$ are the structural mass, damping and stiffness matrices of the bridge; $\mathbf{u}$,$\dot{\mathbf{u}}$,$\ddot{\mathbf{u}}$ denote nodal displacement, velocity and acceleration vectors respectively. $\mathbf{P} = \{P_1(t),P_2(t),...,P_{Np}(t)\}^T$ are vehicle-bridge interaction forces; $\Phi = \{\Phi_1\ \Phi_2...\Phi_l...\Phi_{Np}\}$ is a $2(N+1) \times N_p$ matrix and N is the number of finite element in the bridge structure.

In the inverse problem of damage identification, it is assumed that the stiffness matrix of the whole element decreases uniformly with the damage, and the flexural rigidity, EI_i, of the ith finite element of the beam becomes

$\alpha_i EI_i$ when there is damage. A positive value of $\alpha_i \in [0,1]$ will indicate a loss in the element stiffness. The ith element is undamaged when $\alpha_i = 1$ and the stiffness of the ith element is completely lost when $\alpha_i = 0$. The stiffness matrix of the damaged structure is the assemblage of all the element stiffness matrix

$$\mathbf{K}_{\mathrm{b}} = \sum_{i=1}^{N} \alpha_i \mathbf{A}_i^{\mathrm{T}} \mathbf{K}_{\mathrm{b}i} \mathbf{A}_i, \tag{9}$$

where $\mathbf{A}_i$ is the extended matrix of element nodal displacement that facilitates automatic assembling of global stiffness matrix from the constituent element stiffness matrix.

From Eq. (8), the moving loads can be obtained as follows if the restoring forces are known

$$\mathbf{P} = (\mathbf{\Phi}^{\mathrm{T}}\mathbf{\Phi})^{-1}\mathbf{\Phi}^{\mathrm{T}}[\mathbf{M}_{\mathrm{b}}\ddot{\mathbf{u}} + \mathbf{C}_{\mathrm{b}}\dot{\mathbf{u}} + \mathbf{K}_{\mathrm{b}}\mathbf{u}], \tag{10}$$

The moving loads obtained from Eq. (10) with a straightforward least-squares solution would be unbounded. A regularization technique can be used to solve the ill-posed problem in the form of minimizing the function

$$J(\mathbf{P},\lambda) = \|\mathbf{B}\mathbf{P} - \mathbf{U}\|^2 + \lambda\|\mathbf{P}\|^2, \tag{11}$$

where $\mathbf{B} = \mathbf{\Phi}$ and $\mathbf{U} = \mathbf{M}_{\mathrm{b}}\ddot{\mathbf{u}} + \mathbf{C}_{\mathrm{b}}\dot{\mathbf{u}} + \mathbf{K}_{\mathrm{b}}\mathbf{u}$.$\lambda$ is the nonnegative regularization parameter. And the element damage index matrix is obtained from Eq. (9) after the moving loads are identified from minimizing the following function

$$J(\boldsymbol{\alpha}) = \|F(\mathbf{u}) - K_{\mathrm{b}}\mathbf{u}\|^2, \tag{12}$$

where $F(\mathbf{u}) = \mathbf{\Phi}\mathbf{P}_{\mathrm{identify}}(t) - \mathbf{M}_{\mathrm{b}}\ddot{\mathbf{u}} - \mathbf{C}_{\mathrm{b}}\dot{\mathbf{u}}$; $\mathbf{P}_{\mathrm{identify}}(t)$ is the identified moving loads from Eq. (11).

As the damage index and moving loads are all unknown, the iterative algorithm shown below will be adopted to solve the problem.

1) Calculate the nodal displacements or strains from measurements by Eq. (8);

2) Use the orthogonal function expansion to calculate the nodal velocity and accelerations [27]. Twenty terms in the expansion have been used in this study;

3) Initially assume there is no damage in the beam: $\boldsymbol{\alpha}_0 = \{1,1,...,1\}^{\mathrm{T}}$;

4) Identify the moving loads $\mathbf{P}_{\mathrm{identify}}(t)$ from the measured responses using Eq. (11). Regularization technique is used to stabilize the solution.

5) Calculate the elastic restoring forces,

$$F(\mathbf{u}) = \mathbf{\Phi}\mathbf{P}_{\mathrm{identify}}(t) - \mathbf{M}_{\mathrm{b}}\ddot{\mathbf{u}} - \mathbf{C}_{\mathrm{b}}\dot{\mathbf{u}}, \tag{13}$$

6) Identify the damage index using Eq. (12);

7) Calculate the error for convergence:

$$\begin{cases} \mathrm{Error1} = \dfrac{\|\mathbf{P}_{i+1} - \mathbf{P}_i\|}{\|\mathbf{P}_i\|} \times 100\% \\ \mathrm{Error2} = \dfrac{\|\boldsymbol{\alpha}_{i+1} - \boldsymbol{\alpha}_i\|}{\|\boldsymbol{\alpha}_i\|} \times 100\% \end{cases}, \tag{14}$$

Convergence is achieved when the sum of these two errors is a minimum.

8) When the computed errors do not converge, repeat Steps 4 to 7.

3.2 Numerical examples

A simple example is presented here to the application of this method. The bridge-vehicle system is represented by a simply supported bridge subject to a four DOFs system of moving vehicle as shown in Fig. 6. The parameters of the bridge are:

$$EI = 4.30 \times 10^{10}\,\mathrm{Nm}^2, \rho A = 11000\,\mathrm{kg/m}, L = 60\,\mathrm{m}.$$

The first six natural frequencies of the bridge are 5.23,

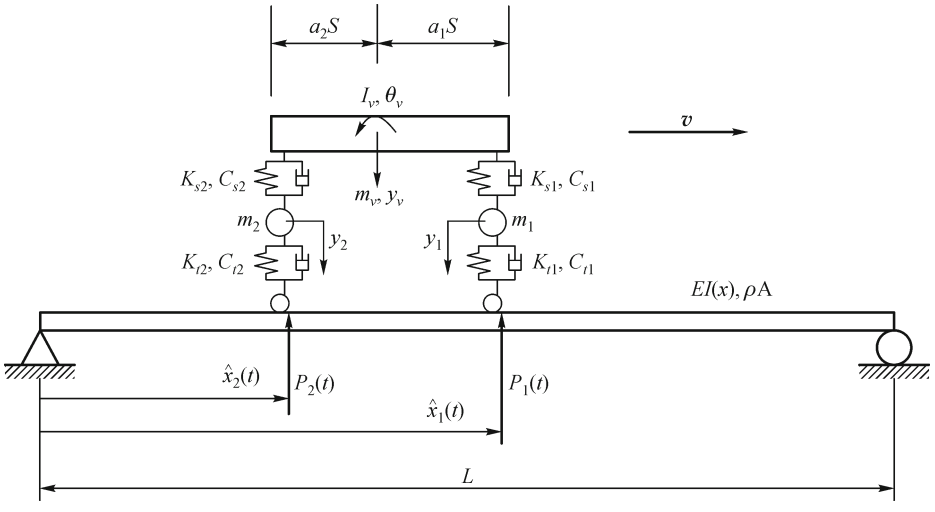

Fig. 6 A vehicle-bridge system

20.56, 48.16, 85.83, 129.80 and 189.73 Hz. The characteristics of the vehicle model are as follows:

$$m_v = 17735\,\text{kg}, m_1 = 1500\,\text{kg},$$

$$m_2 = 1000\,\text{kg}, S = 4.27\,\text{m},$$

$$a_1 = 0.519, a_2 = 0.481,$$

$$H = 1.80\,\text{m}, k_{s1} = 2.47 \times 10^6\,\text{N}\cdot\text{m}^{-1},$$

$$k_{s2} = 4.23 \times 10^6\,\text{N}\cdot\text{m}^{-1}, k_{t1} = 3.74 \times 10^6\,\text{N}\cdot\text{m}^{-1},$$

$$k_{t2} = 4.60 \times 10^6\,\text{N}\cdot\text{m}^{-1},$$

$$c_{s1} = 3.00 \times 10^4\,\text{N}\cdot\text{m}^{-1}\cdot\text{s}, c_{s2} = 4.00 \times 10^4\,\text{N}\cdot\text{m}^{-1}\cdot\text{s},$$

$$c_{t1} = 3.90 \times 10^3\,\text{N}\cdot\text{m}^{-1}\cdot\text{s},$$

$$c_{t2} = 4.30 \times 10^3\,\text{N}\cdot\text{m}^{-1}\cdot\text{s}, I_v = 1.47 \times 10^5\,\text{kg}\cdot\text{m}^2$$

The natural frequencies of the vehicle are 1.63, 2.30, 10.35 and 15.10 Hz. The weight ratio between the vehicle and bridge is 0.135. All these parameters are within the usual range of long span bridge deck. The damage of the beam is in the fifth element with the damage index 0.5. 1%, 5%, and 10% noise is added to the calculated responses to simulate the polluted measurements. The moving loads and damage in the bridge are identified in sequence of iteration from the measurements. The number of the measurements is equal to the number of the elements minus one. The time interval is 0.004 s in the calculation. Figs. 7 and 8 show the identified results with different noise levels in the measurements. The moving speed of the vehicle is 30 m/s. The following observations are made from this study:

The identified results are close to the true values indicating that the method is effective and reliable to identify damage in the bridge structure and the moving loads iteratively from noisy measurements. The identified

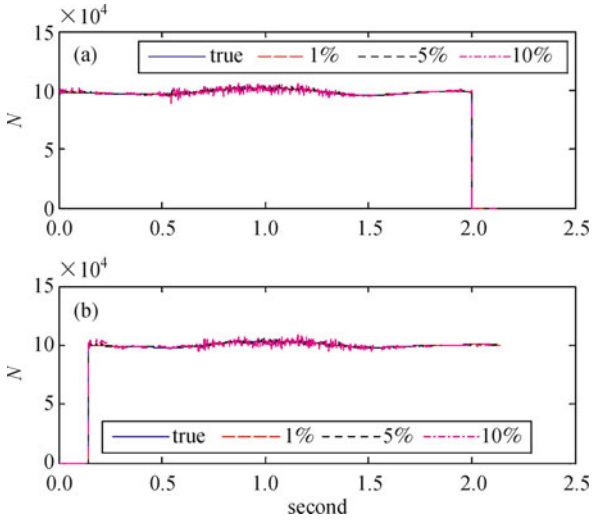

Fig. 7 Identified moving loads. (a) the first axle force; (b) the second axle force

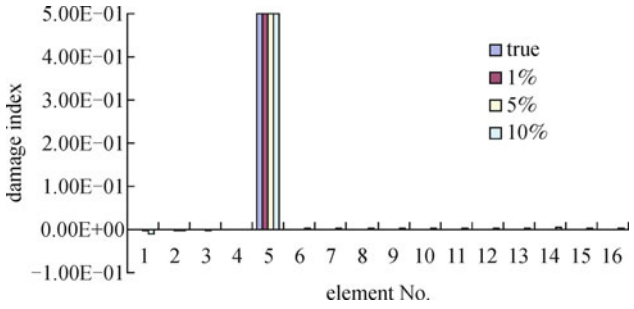

Fig. 8 Identified damage index

results are insensitive to the noise level up to 10%. This is due to the orthogonal function expansion method used to calculate the generalized responses, and the noise in the response is reduced with this approach.

4 Integrated structural evaluation with results from system identification

Structural evaluation has been the ultimate goal of the structural health monitoring practice, but so far little research has been done on this topic. Hosser et al. [28] presented a framework for reliability-based system assessment based on structural health monitoring. The vibration-based identified results are integrated with reliability analysis to yield a safety evaluation of the bridge structure [29]. Soyoz et al. [30] developed a structural reliability estimation method incorporating structural parameter identification results based on the seismic response measurement. In this section, an existing three span concrete bridge is used as the example bridge. The field vibration tests were carried out to obtain modal parameters using 133 measurement locations [31]. The original finite element model of the bridge is built up based on the design drawings and the model is updated using the dynamic filed test data. Finally, the load carrying capacity of the existing bridge is predicted using the updated model.

4.1 Description of bridge No. 852

This over 40 years old slab-on-girder bridge comprises three spans, and 7 girders for each span. Figure 9 shows the dimensions of the bridge deck. The width of the slab is 9.14 m accommodating two traffic lanes. The external span is 17.84 m and the central span is 18.29 m. The girders are precasted as simple beams and then made continuous by placing enough reinforcements in the cast-in-place concrete slab over the support. The slab and girders are integrated by shear connectors as shown Fig. 9. The location of the shear connectors in the girders are illustrated in Fig. 10. The layout of the section in middle of the span is shown in Fig. 9. The prestressing strands are 7-wire stress-relieved high tensile steel strands. They were

released at 123 kN per strand for 84.8 kN design prestressing load per strand. The girders are prefabricated, while the run-on RC slab and diaphragms were casted in place to join the girders. The diaphragms are supported on cap beams measured as 1004 mm × 648 mm for the abutments and 1004 mm × 684 mm for the middle piers. The thickness of the slab is 140 mm on average. Figure 9 shows the reinforcement of the slab in the middle of the span.

4.2 Finite element model

A three-dimensional finite element model (Fig. 11) is built according to the design drawings. The letters A to G indicate the transverse position of the girders and the bearings. The material constitutive models used in the analysis are described in detail by Xia et al. [31] and Hao and Zhu [32].

4.3 Load action for ultimate load carrying capacity evaluation

This bridge was designed based on the old Australian Standards [33,34] nearly 40 years ago. To evaluate the capacity of bridge No. 852 under the action of modern traffic loads, the new traffic loads standard, AS 5100.2-2004, is applied in this study.

Standard AS 5100.2-2004 provides several road traffic loads including single load like the W80 wheel load and

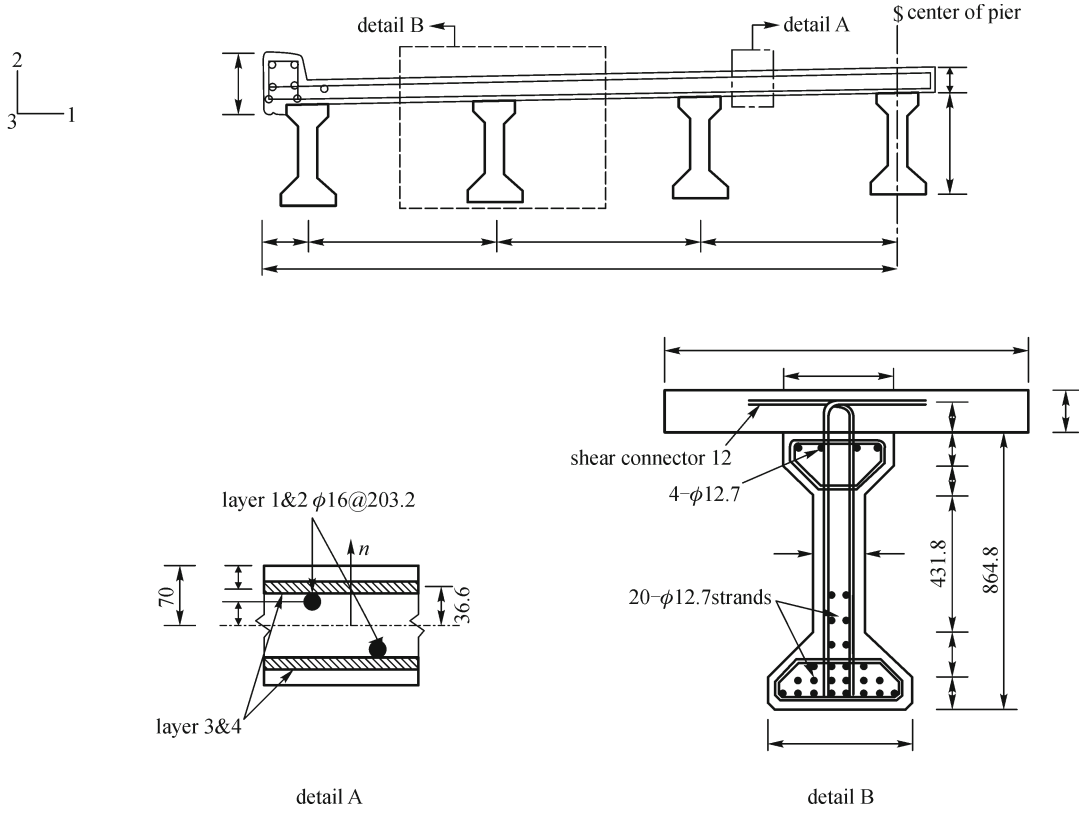

Fig. 9 Dimension of the bridge deck and the reinforcement in the middle of span

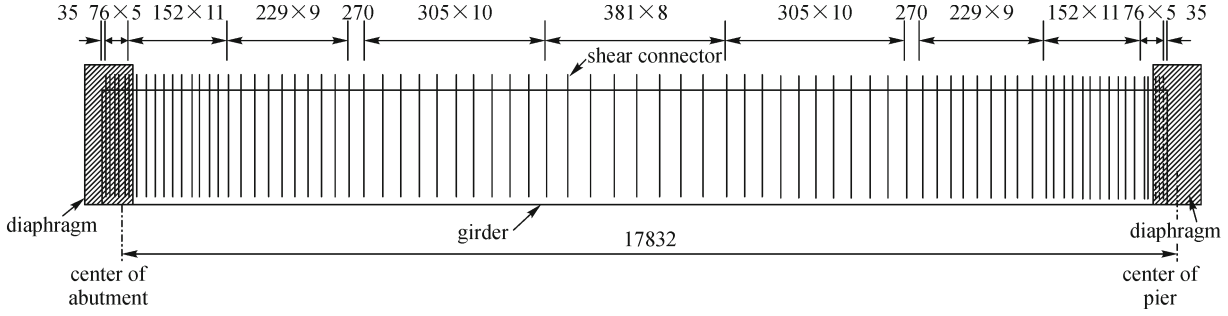

Fig. 10 Location of the shear connectors in one girder

the A160 axle load and group loads like M1600 and S1600. The influence line diagram was used to choose the most critical traffic load combinations and hence to determine the longitudinal positions of the critical loads on the bridge. Then the M1600 traffic loads are selected (see Fig. 12). The M1600 moving traffic load consists of uniformly distributed load together with truck wheel loads. The uniformly distributed load component (UDL) is considered uniformly distributed over the width of a 3.2 m standard design lane (Fig. 12). The wheel loads are treated as concentrated load.

According to the standard AS 5100.2-2004, the width of a standard design lane is 3.2 m. The width of the deck for this bridge between the curbs is 8.5 m. Consequently, two traffic lanes are loaded. The wheel loads for the first lane are located on the second girder to cause the maximum response in this girder. AS 5100.2 requires the minimum clear width for the vehicular traffic is (lane width + 1.2) m. Consequently, the second traffic lane is positioned 1.2 m away from the first lane to produce the maximum moment in the second girder.

The live load effects of the nominated vehicle for load rating, L_{RV} is

$$L_{RV} = \gamma_L(1+\alpha)\sum_{i=1}^{n} W_i S_i^L, \tag{15}$$

where n is the number of the design lane, which equals 2. The live load factor, γ_L is selected as 1.8 (AS 5100.7-2004). W_i is the accompanying lane factor determined in AS 5100.2, which is 1.0 for the first lane and 0.8 for the second lane. The dynamic allowance, α, of 0.3 is considered in the analysis. In this case, the magnitudes of the traffic loads calculated from Eq. (15) are nominated for the load carrying capacity analyses. Furthermore, the nominated rating live load value is equal to the traffic load for an ultimate limit state design (AS 5100.2-2004).

The traffic loads are placed at different places to get the

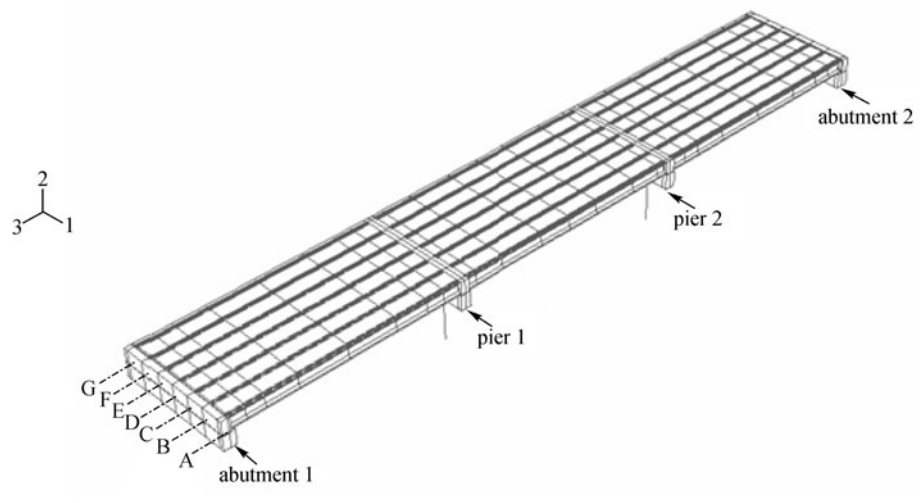

Fig. 11 Finite-element model of Bridge No. 852

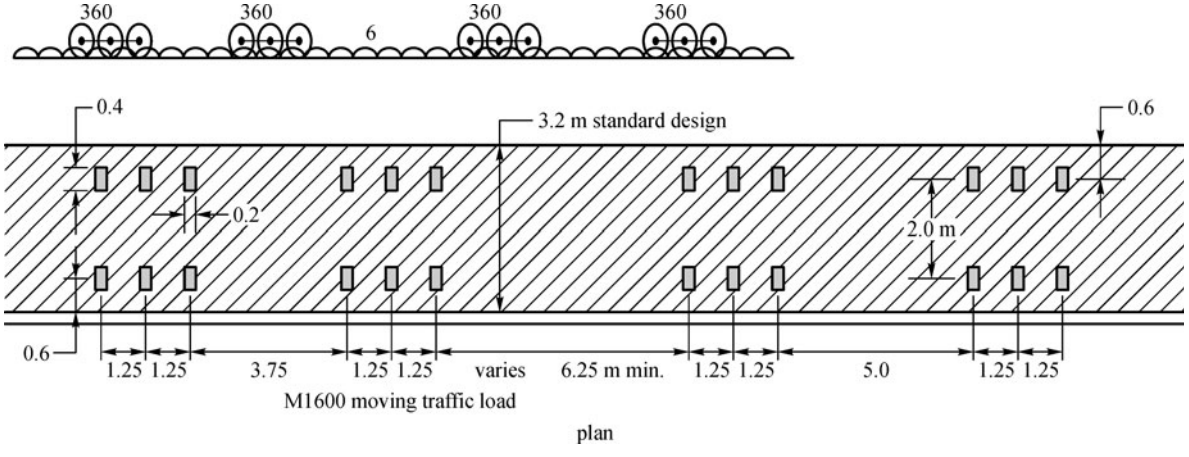

Fig. 12 M1600 moving traffic load

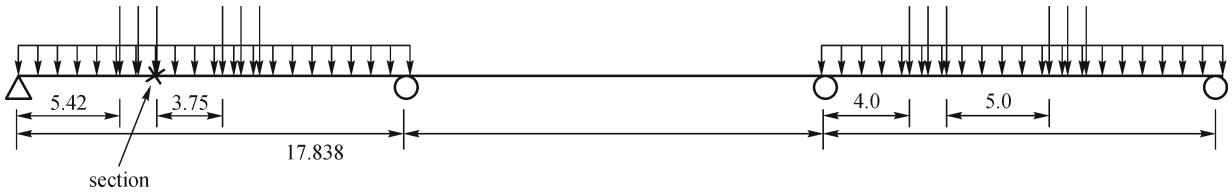

Fig. 13 Longitudinal load position for the most adverse positive moment

most adverse positive and negative moment. Finally, the maximum positive moment is achieved as 7568 kN·m when the first and third spans are loaded, and the minimum negative moment is achieved as −8625 kN·m when the first and second spans are loaded. Compared with the capacity of the bridge calculated from the empirical formula in Sect. 4.1, the bridge capacity is dominated by the positive moment capacity. This bridge can carry 1.39 times of the nominated traffic loads. So the load condition to produce the most adverse positive moment is applied in the following finite element analysis. The positions of the traffic loads are shown in Fig. 13.

4.4 Analysis results

Finite element analysis (FEM) has been carried out to predict the load-displacement curve of the bridge by proportionally increasing the load using ABAQUS. To reflect the actual condition of the bridge, the finite element model has been adjusted using the model updating method with the field test data [35]. Figure 14 shows the comparison of the load displacement curves calculated from the updated model with results from the original model. The vertical axis represents the ratio of the applied load to the nominated rating loads. For the original model, the load-displacement curve can be easily divided into three stages, elastic deformation stage, after cracking, and strands yielding. And the ultimate load carrying capacity is determined by the turning point from increasing to the decreasing of the load. However, for the load-displacement relationship for the updated model, the bridge lost its stiffness at 0.87 of the nominated loads with 53 mm displacement. Then the displacement increased enormously with a little increase of the load. So the turning point A is treated as the maximum load to which the structure can be subjected. It happened before the yielding of the strands. Figure 10 shows the initial stiffness increased by 16% after model updating. The decrease of stiffness in majority of the slab elements is counteracted by the increase of the stiffness in most parts of the girders. For concrete in tension, the plastic strain is defined as the strain minus cracking strain. So the development of cracking can be seen from the contour plot of the plastic strain (PE). In this case, the complete failure mechanism cannot be explained clearly. But from the contour plot of the plastic strain in girder B-1 (Fig. 15) at the moment of the turning point A (in Fig. 14), we can find out that the shear cracks near the support cause the failure of the girder before the cracks developed in the middle of the span.

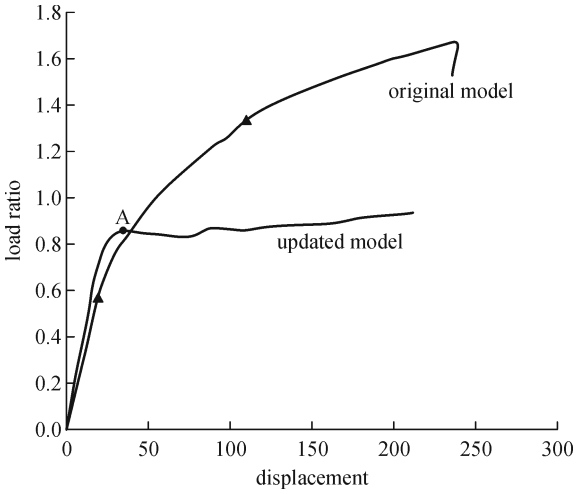

Fig. 14 Load-displacement relationship comparison between original and updated model

5 Conclusions

This paper reports on the development of an integrated structural health monitoring system for bridge structures in operational conditions. It includes integrated sensor technique, integration of structural identification with operational loads monitoring, integrated global and local structural health monitoring, and integration of structural evaluation with the results from system identification. Numerical simulation and its implementation in laboratory show that the system is effective and reliable to detect local damage and global condition of bridge structures. The following conclusions can be obtained,

1) Vibration-based system can be used to monitor the overall structural condition and guide wave based system can be used to detect the localized damage.

2) Structural parameters and operational loads can be identified simultaneously from dynamic response measurements. The identified results can be used to update the structural reliability and service life prediction of existing bridges.

3) The load carrying capacity of existing bridges can be evaluated using the updated finite element model.

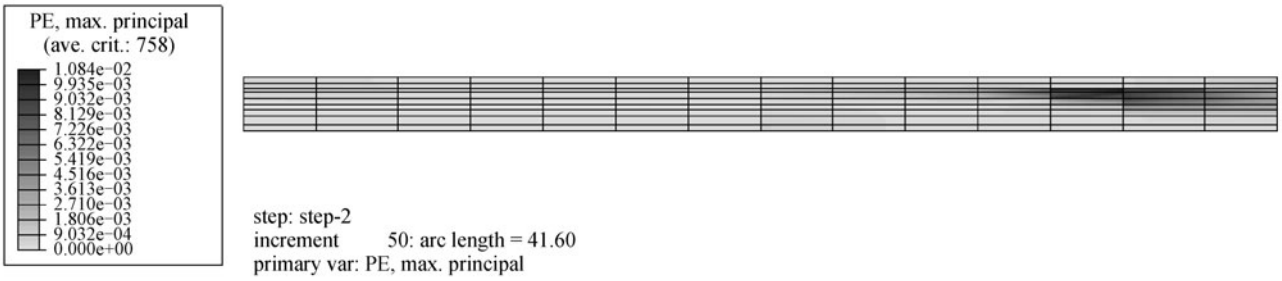

Fig. 15 The plastic strain of girder B-1

In this paper, an integrated structural health monitoring system scheme has been presented. Further study is needed to integrate the local and global approaches and predict the bridge conditions using the results from both the local and global monitoring.

Acknowledgements The work described in this paper was supported by CIEAM II through Project 3104.

References

1. Doebling S W, Farrar C R, Prime M B, Shevitz D W. A review of damage identification methods that examine changes in dynamic properties. Shock and Vibration Digest, 1998, 30(2): 91–105
2. Sohn H, Farrar C R, Hemez F M, Czarnecki J J, Shunk D D, Stinemates D W, Nadler B R. A review of structural health monitoring literature: 1996–2001. Los Alamos National Laboratory Report; LA-13976-MS, 2003
3. Brownjohn JMW. "Structural health monitoring of civil infrastructure." Philosophical Transactions of the Royal Society A: Mathematical, Physical & Engineering Sciences, 2007, 365(1851), 589–622
4. Carden E P, Fanning P. Vibration based condition monitoring: a review. Structural Health Monitoring, 2004, 3(4): 355–377
5. Fan W, Qiao P Z. Vibration-based damage identification methods: a review and comparative study. Structural Health Monitoring, 2011, 10(1): 83–111
6. Brownjohn J M W, de Stefano A, Xu Y L, Wenzel H, Aktan A E. Vibration-based monitoring of civil infrastructure: challenges and successes. Journal of Civil Structural Health Monitoring, 2011, 1(3–4): 79–95
7. Chang P C, Liu S C. Recent research in nondestructive evaluation of civil infrastructures. Journal of Materials in Civil Engineering, 2003, 15(3): 298–304
8. Raghavan A, Cesnik C E S. Review of Guided-wave structural health monitoring. Shock and Vibration Digest, 2007, 39(2): 91–114
9. Kim S D, In C W, Cronin K E, Sohn H, Harries K. Reference-free NDT technique for debonding detection in CFRP-strengthened RC structures. Journal of Structural Engineering, 2007, 133(8): 1080–1091
10. Sohn H, Kim S D, In C W, Cronin K E, Harries K. Debonding monitoring of CFRP strengthened RC beams using active sensing and infrared imaging. Smart Structures and Systems, 2008, 4(4): 391–406
11. Lee S J, Sohn H. Active self-sensing scheme development for structural health monitoring. Smart Materials and Structures, 2006, 15(6): 1734–1746
12. Park G, Cudney H H, Inman D J. An integrated health monitoring technique using structural impedance sensors. Journal of Intelligent Material Systems and Structures, 2000, 11: 448–455
13. Banerjee S, Ricci F, Monaco E, Mal A. A wave propagation and vibration-based approach for damage identification in structural components. Journal of Sound and Vibration, 2009, 322(1–2): 167–183
14. Ratnam C, Ben B S, Ben B A. Structural damage detection using combined finite-element and model lamb wave propagation parameters. Journal of Mechanical Engineering Science, 2009, 223(3): 769–777
15. Zhang J, Xu Y L, Li J. Integrated system identification and reliability evaluation of stochastic building structures. Probabilistic Engineering Mechanics, 2011, 26(4): 528–538
16. Ling Y, Mahadevan S. Integration of structural health monitoring and fatigue damage prognosis. Mechanical Systems and Signal Processing, 2012, 28: 89–104
17. Wang Y, Hao H. Integrated health monitoring for reinforced concrete beams: an experimental study. Australian Journal of Mechanical Engineering, 2011, 8(2): 207–217
18. Zhu X Q, Hao H, Fan K Q, Wang Y, Ou J P. Debond detection of RC structures using piezoelectric materials. In: Proceedings of the International Conference on Concrete Repair, Rehabilitation and Retrofitting, Cape Town, South Africa, 2008
19. Wang Y, Zhu X Q, Hao H, Ou J P. Guided wave propagation and spectral element method for debonding damage assessment in RC structures. Journal of Sound and Vibration, 2009, 324(3–5): 751–772
20. Law S S, Zhu X Q. Damage Models and Algorithms for Assessment of Structures under Operational Conditions. CRC Press: Taylor & Francis Group, 2009
21. Bu J Q, Law S S, Zhu X Q. Innovative bridge condition assessment from dynamic response of a passing vehicle. Journal of Engineering Mechanics, 2006, 132(12): 1372–1379
22. Rafiquzzaman A K M, Yokoyama K. Application of operating

vehicle load to structural health monitoring of bridges. Smart Structures and Systems, 2006, 2(3): 275–293

23. Zhu X Q, Law S S. Damage detection in simply supported concrete bridge structures under moving vehicular loads. Journal of Vibration and Acoustics ASME, 2007, 129(1): 58–65
24. Kim J H, Lynch J P, Lee J J, Lee C G. Truck-based mobile wireless sensor networks for the experimental observation of vehicle-bridge interaction. Smart Materials and Structures, 2011, 20(6): 1–13
25. Hester D, Gonzalez A. A wavelet-based damage detection algorithm based on bridge acceleration response to a vehicle. Mechanical Systems and Signal Processing, 2012, 28: 145–166
26. Zhu X Q, Hao H. Dynamic assessment of highway bridges using operating vehicle loads. In: Proceedings of the 6th International Workshop on Structural Health Monitoring, Stanford, CA, 11–13 September 2007
27. Zhu X Q, Law S S. Orthogonal function in moving loads identification on a multi-span bridge. Journal of Sound and Vibration, 2001, 245(2): 329–345
28. Hosser D, Klinzmann C, Schnetgoke R. A framework for reliability-based system assessment based on structural health monitoring. Structures and Infrastructure Engineering, 2008, 4(4): 271–285
29. Law S S, Li J. Updating the reliability of a concrete bridge structure based on condition assessment with uncertainties. Engineering Structures, 2010, 32(1): 286–296
30. Soyoz S, Feng M Q, Shinozuka M. Structural reliability estimation with vibration-based identified parameters. Journal of Engineering Mechanics, 2010, 136(1): 100–106
31. Xia Y, Hao H, Deeks A J, Zhu X Q. Condition assessment of a full slab-girder bridge via vibration measurements. Journal of Bridge Engineering, 2008, 13(1): 43–54
32. Hao H, Zhu X Q. Dynamic assessment of PSC bridge structures under moving vehicular loads. In: Proceedings of the International Workshop on “Civil Structural Health Monitoring 2”: WIM (weigh in motion), Load Capacity and Bridge Performance, Taomina, Italy, 2010b
33. Australian Standard. Bridge Design Part 2: Design loads (AS5100.2). Sydney: Standards Australia International Ltd., 2004
34. Australian Standard. Bridge Design Part 7: Rating of existing bridges (AS5100.7). Sydney: Standards Australia International Ltd, 2004
35. Ding L N. Bridge Load Rating with Model Updating and Stochastic Analysis of Vehicle-Bridge Interaction. The PhD Thesis of the University of Western Australia, 2010
36. Hao H, Zhu X Q. Development of an integrated structural health monitoring system for civil infrastructure under operational environments. In: Proceedings of the International Workshop on “Civil Structural Health Monitoring 2”: WIM (weigh in motion), Load Capacity and Bridge Performance, Taomina, Italy, 2010a